DOI: 10.1002/ejic.200500474

A Crystalline Phase Transition and Optical Properties in a $Co^{II}Cu^{II}$ Oxamato-Bridged Ferrimagnetic Chain

Cynthia L. M. Pereira,[a] Antonio C. Doriguetto,[b] Cibele Konzen,[c] Luiz C. Meira-Belo,[c] Ulisses A. Leitão,[d] Nelson G. Fernandes,[a] Yvonne P. Mascarenhas,[b] Javier Ellena,[b] Ana L. Brandl,[e] Marcelo Knobel,[e] and Humberto O. Stumpf*[a]

Keywords: Birefringence / Chain structures / Molecular magnetism / Phase transitions / Transition metals

The compound [CoCu(opba)$(DMSO)_3$] (**1**) [opba = *ortho*-phenylenebis(oxamato)] has been synthesized and characterized. Its crystal structure has been analyzed by X-ray diffraction techniques at 100 and 298 K. A structural phase-transition has been detected at around 150 K. An orthorhombic crystalline system is found at both temperatures, with very similar unit-cell dimensions. At room temperature **1** crystallizes in the *Pnam* space group (**α-1** phase), with a = 7.6712(2), b = 14.8003(3), c = 21.0028(5) Å, and Z = 4, whereas at low temperature it crystallizes in the $Pna2_1$ space group (**β-1** phase), with a = 7.3530(2), b = 14.5928(4), c = 21.0510(7) Å, and Z = 4. Both crystalline phases consist of linearly ordered bimetallic chains with the $[Cu(opba)]^{2-}$ units tied by Co^{II} ions to form a one-dimensional system. The DMSO molecules in **α-1**, which are coordinated to either Cu^{II} or Co^{II}, are disordered. At low temperature, a small reorganization of the Cu^{II} and Co^{II} environments is observed. The origin of this phase transition, which is completely reversible, is the modification of the crystalline packing with the temperature. Linear birefringence measurements were done on single crystals in the 100–300 K temperature range. Around 150 K, the linear birefringence curve shows an inflexion that is interpreted as being related to the conversion of **α-1** into **β-1**. Both dc and ac magnetic measurements were performed on the polycrystalline sample. The results reveal a one-dimensional ferrimagnetic behavior. Single crystal optical characterization at room temperature shows that **1** presents a very strong dichroism superposed on the linear birefringence.

Introduction

The first molecule-based magnets described were the organometallic compound $[Fe(Me_5Cp)_2][TCNE]$ (Me_5Cp = pentamethylcyclopentadienyl; TCNE = tetracyanoethylene)[1] and the chain $[MnCu(pbaOH)(H_2O)_3]$ [pbaOH = 2-hydroxy-1,3-propylenebis(oxamato)].[2] Since then, there has been a rapid development of this field of research, with special focus on the design of materials with predictable magnetic properties and potential technological applications.[3–5] In the last two decades, the chemistry of molecular magnetic materials has been widely exploited in two branches. In the first one, the key goal is to optimize the magnetic properties by increasing the Curie temperature, coercivity, spin transition, blocking temperature, or tunneling effects,[6–11] whereas in the second branch the focus is on aggregating other characteristics to the magnetic materials, such as optical properties or conductivity.[12–14] What these two branches have in common is the employment of molecular chemistry in a bottom-up strategy. Let us illustrate this using the oxamato-bridged system as an example. One of the first steps of this approach consists in synthesizing a building block like $[Cu(opba)]^{2-}$ [Figure 1; opba = *ortho*-phenylenebis(oxamato)].[15] This precursor possesses two lone pairs on either side of the peripheral oxygen atoms and therefore it may behave as a bis-bidentate ligand. The next stage is the choice of a metal ion whose characteristics must induce the production of a material with desirable properties. Supramolecular aspects can become very impor-

[a] Departamento de Química, ICEx, Universidade Federal de Minas Gerais,
Av. Antônio Carlos 6627, Pampulha, Belo Horizonte, MG, 31270-901, Brazil
Fax: +55-31-3499-5700
E-mail: stumpf@ufmg.br
[b] Instituto de Física de São Carlos, Universidade de São Paulo, C. P. 369, São Carlos, SP, 13560-970, Brazil
Fax: +55-16-273-9881
E-mail: dorigue@if.sc.usp.br
[c] Laboratório de Física Aplicada, Centro de Desenvolvimento da Tecnologia Nuclear,
C. P. 941, BH, MG, 30932-970, Brazil
Fax: +55-31-3499-3390
E-mail: lcmb@cdtn.br
[d] Departamento de Física, ICEx, Universidade Federal de Minas Gerais,
Av. Antônio Carlos 6627, Pampulha, BH, MG, 31270-901, Brazil
Fax: +55-31-3499-5700
E-mail: uli@fisica.ufmg.br
[e] Instituto de Física Gleb Wataghin, Universidade Estadual de Campinas,
C. P. 6165, 13083-970, Campinas, SP, Brazil
Fax: +55-19-3788-5480
E-mail: knobel@ifi.unicamp.br
Supporting information for this article is available on the WWW under http://www.eurjic.org or from the author.

tant in this step. Besides the stoichiometric ratios, concentration, and counterion nature, the solvent can play a key role. Indeed, the first chain to be synthesized using this precursor was [MnCu(opba)$(DMSO)_3$], which was obtained in DMSO.[15] This compound has an unexpected zigzag chain structure with two DMSO molecules bound to the manganese atom in a *cis* fashion. [MnCu(opba)$(DMSO)_3$] is an almost perfect one-dimensional ferrimagnet where the chains are isolated by DMSO molecules in the crystalline packing. When the reaction is performed in a DMSO/H_2O mixture, the octahedral environment of the Mn^{II} is completed by two water molecules in *trans* positions and the product obtained, [MnCu(opba)$(H_2O)_2$]·DMSO, consists of linear chains.[16] In this latter compound, the chains interact weakly within the crystal lattice and the compound shows an antiferromagnetic transition with T_N = 5 K and metamagnetic behavior. By making some changes we can prepare 2D, graphite-like compounds with the general formula $[cat]_2[M_2\{Cu(opba)\}_3]$[15,17] or interlocked systems[6,18,19] where the counterion cat^+ is a nitronyl-nitroxide radical cation. Very recently, a new class of bidimensional metallacyclophane-based compounds $[Co_2Cu_2(mpba)_2(H_2O)_6]\cdot 6H_2O$ [mpba = *meta*-phenylenebis(oxamato)], which present a corrugated brick-wall structure, have been obtained.[20]

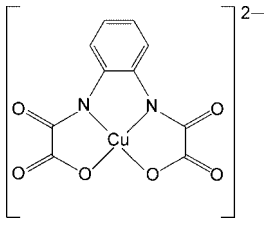

Figure 1. Building block $[Cu(opba)]^{2-}$.

The aim in preparing these 2D and 3D molecule-based systems was to increase the critical temperatures of the magnetic ordering. With the report of the [$Co(hfac)_2$NITPhOMe] nanowire, which shows slow relaxation of the magnetization and hysteretic effects, by Gatteschi et al.,[21] a renewed interest in linear systems has emerged. In this paper, we will describe the synthesis, structure, and magnetic and optical properties of the chain [CoCu(opba)$(DMSO)_3$] (**1**). Furthermore, a study of the linear birefringence measurements and single-crystal X-ray crystallography in order to confirm a temperature-induced crystalline phase-transition for **1** will be presented.

Results and Discussion

Crystal Structures of [CoCu(opba)$(DMSO)_3$] Phases

X-ray diffraction experiments were carried out at two different temperatures (298 and 100 K). The structures of **α-1** and **β-1** are shown in Figure 2. In both cases the structure consists of ordered infinite linear chains running along the *c* axis with adjacent Co^{II} and Cu^{II} ions bridged by oxamato groups. This compound does not have the zigzag structure of [MnCu(opba)$(DMSO)_3$];[15] it is more similar to the linear chain of [MnCu(opba)$(H_2O)_2$]·DMSO.[16] However, in contrast to this latter chain, the aromatic rings of **1** are alternately on one and the other side of the chain axis.

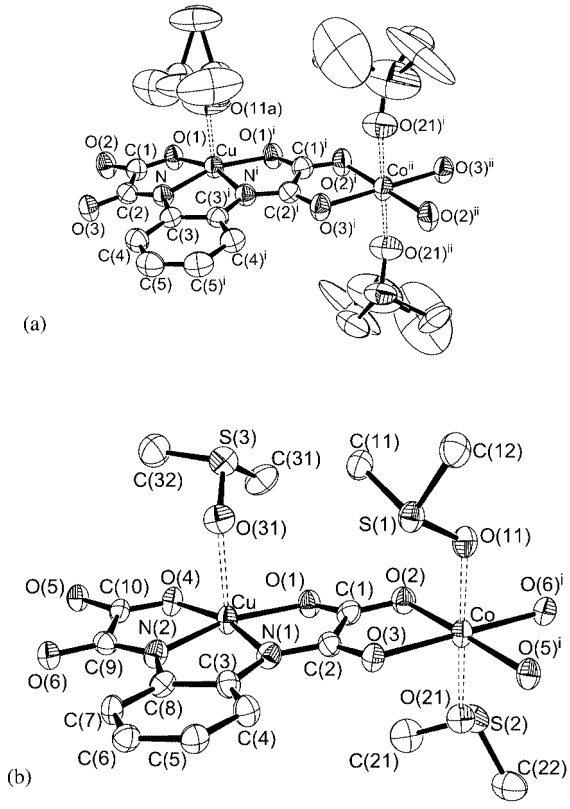

Figure 2. ORTEP3 drawing of the phases **α-1** (a) and **β-1** (b) of the chain [CoCu(opba)$(DMSO)_3$] (**1**) showing some atom designation. The thermal ellipsoids are drawn at the 50% probability level.

The main geometric parameters for phases **α-1** and **β-1** are given in Table 1. It is important to emphasize that **α-1** has half as many independent atoms as **β-1** due to its extra inversion center.

The geometry around the copper atom is approximately square pyramidal with two nitrogen atoms and two oxygen atoms from the opba group in the basal plane and one DMSO oxygen atom in the apical position. The DMSO molecules bonded to the Cu ions are disordered in **α-1**. This disorder disappears at low temperature, and a subsequent phase transition occurs to give **β-1**. In the phase **α-1**, the two N–Cu–O fragments present identical geometry due to their mirror symmetry. The $[Cu(opba)]^{2-}$ unit geometry is not analogous to those previously found for $Mn^{II}Cu^{II}$ bimetallic compounds either for **α-1** or **β-1**.[15,16]

The cobalt atom is coordinated to six oxygen atoms in a distorted octahedral surrounding. Two of these oxygen atoms, arising from the DMSO molecules, are in *trans* positions; the other four belong to oxamido groups of two different opba ligands. Similar to the Cu coordination sphere, the DMSO molecules coordinated to the Co atoms are disordered in **α-1**, whereas no disorder is observed in the **β-1** phase. In **α-1**, the Co ions are located on the inversion center. Therefore, only two of four opba oxygen atoms and one

Table 1. Main geometric parameters (Å, °) for **1**.[a]

Phase **α-1**		Phase **β-1**	
Cu–N	1.921(3)	Cu–N(2)	1.908(5)
		Cu–N(1)	1.937(5)
Cu–O(1)	1.994(2)	Cu–O(1)	2.002(4)
		Cu–O(4)	2.005(4)
Cu–O(11A)	2.19(3)	Cu–O(31)	2.333(5)
Co^{i}–$O(2)^{i}$	2.083(2)	Co–O(2)	2.120(4)
Co^{i}–$O(3)^{i}$	2.074(2)	Co–O(3)	2.052(4)
		Co–$O(5)^{i}$	2.105(4)
		Co–$O(6)^{i}$	2.044(4)
Co^{i}–$O(21)^{i}$	2.123(3)	Co–O(11)	2.103(4)
		Co–O(21)	2.141(4)
$N–C_{(mean)}$	1.36(7)	$N–C_{(mean)}$	1.36(6)
$O–C_{(mean)}$	1.25(1)	$O–C_{(mean)}$	1.26(1)
C(1)–C(2)	1.549(5)	C(1)–C(2)	1.539(8)
		C(9)–C(10)	1.540(8)
$C–C_{Ar(mean)}$	1.39(1)	$C–C_{Ar(mean)}$	1.39(2)
		$S–O_{(mean)}$	1.52(1)
		$S–C_{(mean)}$	1.77(2)
N(1)–Cu–O(1)	83.7(1)	N(1)–Cu–O(1)	83.6(2)
		N(2)–Cu–O(4)	83.4(2)
N–Cu–N^{i}	82.5(2)	N(1)–Cu–N(2)	82.5(2)
N–Cu–O(11a)	101.1(6)	N(1)–Cu–O(31)	98.3(2)
		N(2)–Cu–O(31)	99.5(2)
O(1)–Cu–O(11a)	92.8(5)	O(1)–Cu–O(31)	89.8(2)
		O(4)–Cu–O(31)	89.5(2)
$O(2)^{i}$–Co^{ii}–$O(21)^{i}$	90.5(1)	O(2)–Co–O(11)	92.5(2)
$O(3)^{i}$–Co^{ii}–$O(21)^{i}$	88.8(1)	O(3)–Co–O(11)	93.1(2)
$O(2)^{i}$–Co^{ii}–$O(21)^{ii}$	89.5(1)	$O(5)^{i}$–Co–O(11)	90.3(2)
$O(3)^{i}$–Co^{ii}–$O(21)^{ii}$	91.2(1)	$O(6)^{i}$–Co–O(11)	88.5(2)
		O(2)–Co–O(21)	86.7(2)
		O(3)–Co–O(21)	88.8(2)
		$O(5)^{i}$–Co–O(21)	90.5(2)
		$O(6)^{i}$–Co–O(21)	89.6(2)
$O(2)^{i}$–Co^{ii}–$O(3)^{i}$	81.43(9)	O(2)–Co–O(3)	80.8(2)
		O(2)–Co–$O(6)^{i}$	97.3(2)
$O(3)^{i}$–Co^{ii}–$O(2)^{ii}$	98.57(9)	O(3)–Co–$O(5)^{i}$	100.3(2)
		$O(5)^{i}$–Co–$O(6)^{i}$	81.6(2)
		$C–S–C_{(mean)}$	97(1)
		$O–S–C_{(mean)}$	106(1)
$C(2)–N–Cu_{(mean)}$	115.3(7)	$C–N–Cu_{(mean)}$	115.4(5)
C(1) –O(1) –Cu	111.2(2)	C(1)–O(1)–Cu	110.4(4)
		C(10)–O(4)–Cu	110.9(4)
$C–O–Co_{(mean)}$	111.4(9)	$C–O–Co_{(mean)}$	111.7(4)
		S(1)–O(11)–Co	122.8(2)
		S(2)–O(21)–Co	122.1(2)
		S(3)–O(31)–Cu	133.9(2)
$O–C–C_{(mean)}$	117.8(9)	$O–C–C_{(mean)}$	117.6(9)
$N–C–C_{(mean)}$	112(2)	$N–C–C_{(mean)}$	112(1)
$C–C–C_{Ar(mean)}$	120(1)	$C–C–C_{Ar(mean)}$	120.0(6)

[a] Symmetry codes: phase **α-1**: [i] *x*, *y*, –*z* + 1/2; [ii] *x*, –*y* + 1, *z* + 1/2; phase **β-1**: [i] –*x*, –*y* + 1, *z* + 1/2.

of the two DMSO oxygen atoms are independent. In spite of this, the geometric parameters of the Co octahedron do not exhibit significant differences when the two phases are compared (see Table 2).

Both phases have very similar packing in which each chain is surrounded by six others (see Figure 3).[22] The shortest metal–metal distances (approx. 5.3 Å) occur between intrachain nearest neighbor Cu^{II} and Co^{II} ions. In **α-1** there is just one independent Cu···Co intrachain separation [5.303(1) Å], whereas in **β-1** there are two symmetrically independent intrachain Cu···Co contacts with distances equal to 5.336(1) (Cu···Co) and 5.305(1) Å (Cu···Co^{ii}; *ii* = –*x*, –*y* + 1, *z* – 1/2). The separation between adjacent chains along the *a* axis is exactly equal to the length of the cell parameter in this direction. This means that interchain Co···Co^{i} and Cu···Cu^{i} (*i* = *x* + 1, *y*, *z*) distances along the *a* axis are equivalent and decrease by about 0.3 Å from **α-1** to **β-1**. The interchain metal–metal separations considering transverse adjacent chains show significant differences between the **α-1** and **β-1** phases, mainly with respect to the Co···Co distances. For **α-1** there is just one independent transversal Co···Co distance [8.335(1) Å] since the Co atom is in the special position (0, 0, 1/2). For **β-1** the Co atom is shifted from the unit-cell edges mainly for the *z* coordinate. Therefore, the Co···Co distance is split in two: [Co···Co^{vi} = 7.818(1) Å (*vi* = *x* + 1/2,–*y* + 1/2, *z*) and Co···Co^{vii} = 8.526(1) Å (*vii* = *x* + 1/2,–*y* + 3/2, *z*)]. Due to the waving of the chain along the *c* axis, the structure presents two very different interchain Cu···Cu separations among transverse adjacent chains. One of them is the shortest metal–metal interchain separation [Cu···Cu^{v} = 7.108(1) Å for **α-1** (*v* = *x* + 1/2, –*y* + 3/2, –*z* + 1/2) and Cu···Cu^{vii} = 6.965(1) Å for **β-1** (*vii* = *x* + 1/2, –*y* + 3/2, *z*)], and the other one is the longest metal–metal first-neighbor separation [Cu···Cu^{iv} = 9.614(1) Å (*iv* = *x* + 1/2, –*y* + 1/2, –*z* + 1/2) for **α-1** and Cu···Cu^{vi} = 9.424(1) Å for **β-1** (*vi* = *x* + 1/2, –*y* + 1/2, *z*)]. The Cu···Co interchain distances range

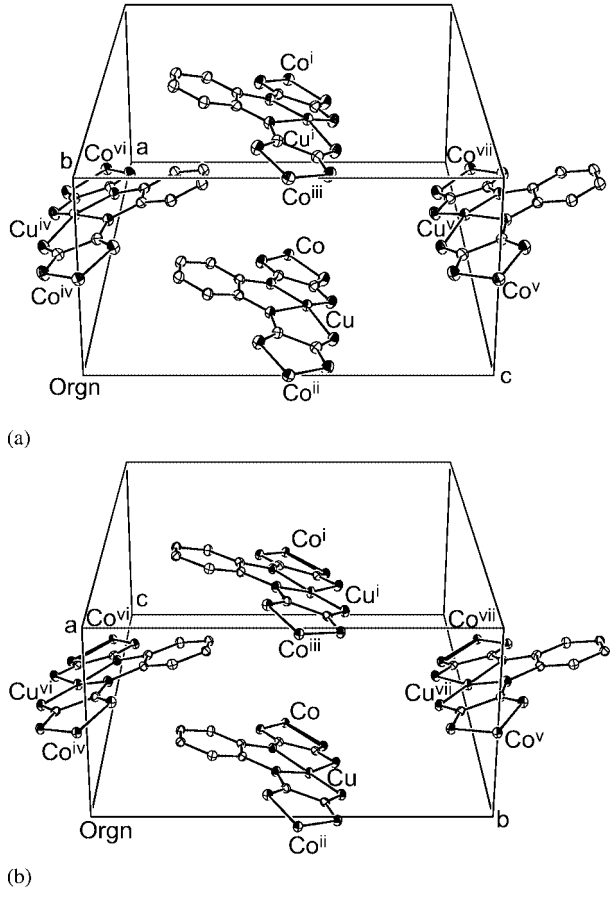

Figure 3. Packing diagram showing the unit cell and the chain neighborhood of the phases **α-1** (a) and **β-1** (b).

Table 2. Crystal data, data collection, and structure-refinement parameters for **1**.

	Phase **α-1** (298 K)	Phase **β-1** (100 K)
Formula	$C_{16}H_{22}N_2O_9S_3CoCu$	
Fw [g mol^{-1}]	605.01	
Crystal system	orthorhombic	
λ (Mo-K_α)	0.71073	
Z	4	
Crystal size [mm]	0.03 × 0.08 × 0.09	
Space group	*Pnma*	*Pna*2$_1$
a [Å]	7.6712(2)	7.3530(2)
b [Å]	14.8003(3)	14.5928(4)
c [Å]	21.0028(5)	21.0510(7)
Volume [Å^3]	2384.6(1)	2258.8(1)
$D_{calcd.}$ [g cm^{-1}]	1.685	1.779
Absorption coefficient [mm^{-1}]	1.898	2.004
F(000)	1232	1232
θ range for data collection [°]	$2 \le \theta \le 50$	$2 \le \theta \le 50$
Index ranges	$-9 \le h \le 9$	$-8 \le h \le 8$
	$-17 \le k \le 17$	$-17 \le k \le 17$
	$-24 \le l \le 24$	$-24 \le l \le 24$
Reflections collected	23067	19898
Independent reflections	3934 [R_{int} = 0.043]	3702 [R_{int} = 0.064]
Data / parameters	2152 / 208	3702 / 290
Max. / min. transmission	0.9111 / 0.8786	0.9064 / 0.8725
Goodness-of-fit on F^2	1.171	1.111
Final *R* indices [$I > 2\sigma(I)$]	R_1 = 0.039, wR_2 = 0.099	R_1 = 0.042, wR_2 = 0.102
R indices (all data)	R_1 = 0.049, wR_2 = 0.105	R_1 = 0.049, wR_2 = 0.107
Largest diff. peak and hole	0.624 & –0.343 e Å^{-3}	0.455 & –0.678 e Å^{-3}

from 9.134(1) to 10.481(1) Å for **α-1** and from 8.752(1) to 10.546(1) Å for **β-1**. For both phases, the shortest contact takes place between parallel chains stacking along the *a* axis. Comparing the two phases, the biggest split due to the inversion symmetry break occurs for the Cu···Co^{i} and Cu···Co^{iii} distances, which are equal to 9.513(1) Å for **α-1** and decrease to 9.256(1) and 8.752(1) Å, respectively, for **β-1**.

Since *Pnam* (**α-1**) differs from *Pna*2$_1$ (**β-1**) only in the extra inversion symmetry in the former, there is no additional peak in the low-temperature diffraction pattern. Due to the reversibility, the phase transition involves only small changes in the atomic positions. This is true for the $[Cu(opba)]^{2-}$ unit and the Co atom. In spite of the fact that the Co ions leave the inversion center on going from phase **α-1** to phase **β-1**, the chains are very similar in both phases. On the other hand, the orientations of the DMSO molecules change significantly between the two phases. With

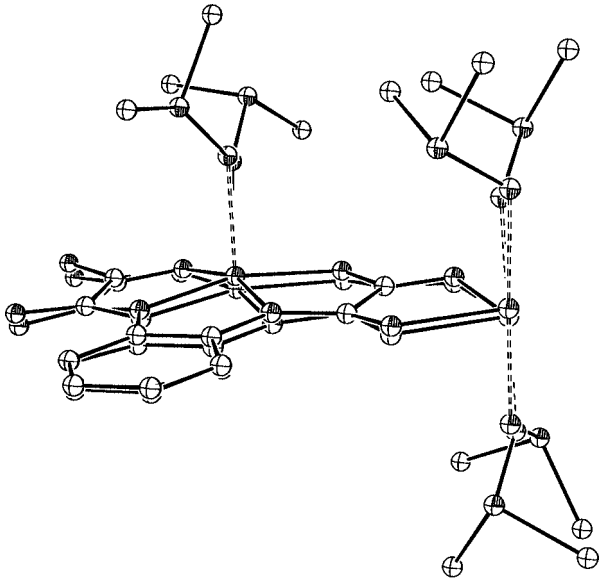

Figure 4. ORTEP3 representation showing a superposition of the molecular structures of **α-1** and **β-1** phases (mechanism 1).

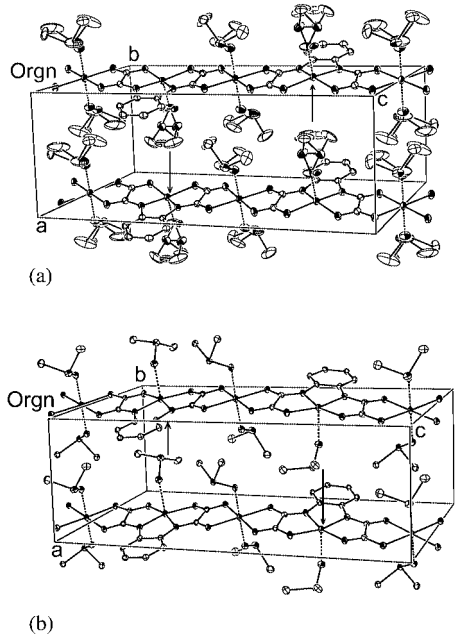

Figure 5. Packing diagram showing two parallel chains along the *b* axis. Arrows indicate the Cooper's DMSO path during the phase transition. Phase **α-1** (top) and phase **β-1** (bottom).

these results in mind, two DMSO ordering mechanisms have been proposed to explain the structural transition. Initially, it was considered that all DMSO molecules could suffer a rotation of 180° around its O–S bond, as depicted in Figure 4 (mechanism 1), where both **α-1** and **β-1** crystalline phases are superposed. However, comparing the packing of the two phases (Figure 5), it is possible to conclude that mechanism 1 should not be the most plausible due to the steric hindrance effects. The most probable is that the DMSO molecule coordinated to the Cu^{II} ion migrates from a chain to another parallel one whilst maintaining almost the same orientation (Figure 5; mechanism 2). Therefore, the DMSO molecule ordering from 298 to 100 K occurs concomitantly with the displacement of DMSO molecules bonded to the Cu ions, with the DMSO groups bonded to the Co ions remaining in almost the same place.

Optical Properties

In order to verify optical anisotropy effects, namely linear birefringence (LB) and linear dichroism (LD), the sample was placed between crossed polarizers. Upon rotating the sample relative to the polarizers, points of extinction were noticed at 90°. Both effects, LB and LD, could be responsible for the observed optical behavior. Upon removing one polarizer we noted extinction points at 180°, thus revealing the LD effect in the sample. The photographic records of these results are available as Supporting Information.

The temperature dependence of the LB is dominated by small differences in the thermal expansion coefficients of the lattice parameters, as shown in Figure 6. This gives rise to an almost linear temperature-dependence behavior, except for the anomalies in the LB. This kind of anomaly is typical of a first-order structural phase transition. A large thermal hysteresis of about 70 K was observed.

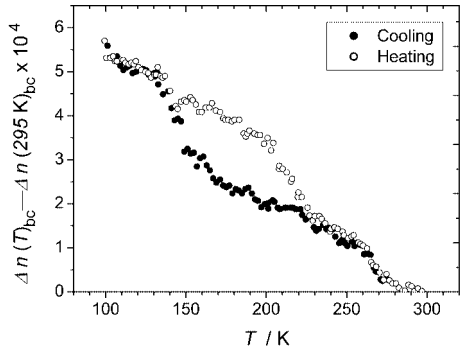

Figure 6. Cooling (solid circles) and heating (open circles) runs of the linear birefringence thermal dependence for **1**.

The optical properties assigned to the structural symmetry of transparent crystals can be described by their characteristic indicatrix, an ellipsoid on phase space of the refraction indices.[23] Orthorhombic crystals have three different values for the axes of its indicatrix, with two circular central sections characterizing a biaxial system, i.e., the crystal has two optical axes. Although both symmetry point groups for **α-1** and **β-1** are orthorhombic, their tensorial properties are different, which became evident by the changes in the birefringence curve on both runs.

The temperature dependence of the LD for **1** was obtained by using a lock-in detector technique analogous to the LB experiment, except for the removal of the analyzer polarizer.[24] The data were collected in the 20–295 K temperature range and the sample was oriented at 45° in order to maximize the LD signal. No significant variation of the lock-in amplifier signal was detected upon maintaining the LD approximately constant during the whole experiment.

Magnetic Studies

The temperature dependence of the magnetic susceptibility for **1** is shown in Figure 7 in the form of a $\chi_M T$ vs. T plot, with χ_M being the molar magnetic susceptibility and T the temperature. At 300 K, $\chi_M T$ (2.87 emu K mol^{-1}) corresponds to what is expected for uncoupled Co^{II} and Cu^{II} ions.[25] At high temperatures, a spin S, of 3/2 can be assigned for Co^{II} ions. As T is lowered, $\chi_M T$ decreases smoothly and reaches a rounded minimum around 90 K with $\chi_M T$ = 2.31 emu K mol^{-1}, and then increases as T is lowered further. Such behavior is characteristic of one-dimensional ferrimagnetism. This decrease of $\chi_M T$ could be due to the spin-orbit coupling effect of octahedral Co^{II} ion,[26] but it is strong enough to confirm the presence of antiferromagnetic coupling between near neighbors, as expected for oxamato-bridged compounds.[27] As T is lowered further below the minimum of $\chi_M T$, the correlation length within the chain increases rapidly. At very low temperatures, the Co^{II} ion behaves as an effective spin of 1/2, but the different g value with respect to the Cu^{II} centers ensures that the ground state will be magnetic.[28]

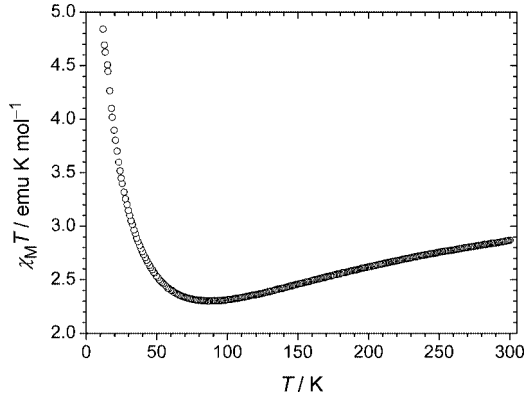

Figure 7. Temperature dependence of $\chi_M T$ for **1** at 1 kOe.

The temperature dependence of the magnetization for **1** is shown in Figure 8. The field-cooled magnetization (FCM), recorded by cooling the sample under a field of 100 Oe, shows a continuous increase, and reaches a value of 600 emu Oe mol^{-1} at 2 K. The zero-field cooled magnetization (ZFCM, not shown) was measured by cooling the sample without an applied field, then warming up under

a 100 Oe field. ZFCM and FCM are coincident, thereby revealing the absence of remnant magnetization.

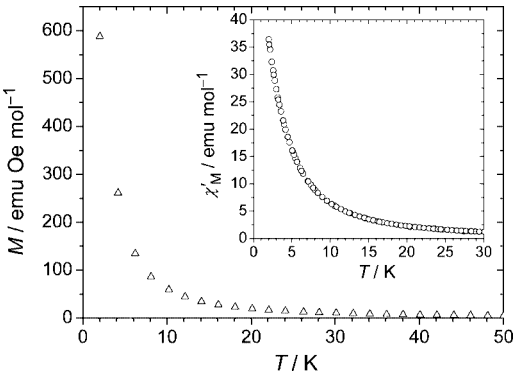

Figure 8. Field-cooled magnetization (FCM) in an applied field of 100 Oe. Inset: Real (χ_M') component of the ac magnetic susceptibility at a frequency of 1 kHz.

The thermal dependence of the in-phase (χ_M') and out-of-phase (χ_M'') components of the ac magnetic susceptibility were also investigated. The χ_M' results at an ac field of 10 Oe measured at 1 kHz and no dc field applied (inset of Figure 8) are very similar to the FCM curve with a rapid increase below 4 K. The χ_M'' curves are close to zero in the investigated temperature range.

Figure 9 shows the field dependence of the magnetization at 2 K for the chain **1**. As the applied field increases, M increases, and does not saturate even for fields as high as 65 kOe, where it reaches a value of 1.4 μ_B mol^{-1} (Nβ). The saturation magnetization is expected to be higher than 2 Nβ, a value related to all S_{Co} local spins aligned along the field direction and all the S_{Cu} local spins aligned along the opposite direction.[25,27] The difference between these values indicates that the local magnetic moments do not reach a perfect alignment with the field direction. This is probably due to the anisotropy of the spin carriers, which prevents the magnetic moments from rotating freely when applying the field. Such behavior is typical for oxamato-based magnets containing Co^{II} ions. No magnetic hysteresis is observed for this compound, even at 2 K (inset of Figure 9).

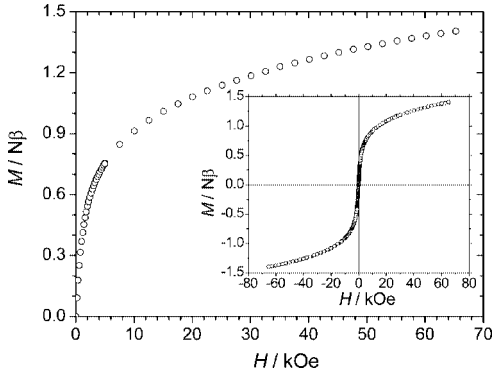

Figure 9. Molar magnetization vs. applied magnetic field for **1** at 2 K. Inset: Hysteresis loop at 2 K.

Let us now briefly discuss the relationship between structure and magnetic properties for **1**. The high-temperature behavior of the magnetic properties is widely dominated by the intrachain couplings along the c axis (J_c or J_{CoCu}). The mechanism of these M^{II}–Cu^{II} interactions (M being a transition metal ion) through the oxamato bridge is rather well understood. These interactions are due to the overlap of the $d_{x^2-y^2}$ magnetic orbitals centered on adjacent spin carriers. The strong covalent bonds and electron delocalization in molecule-based magnets with ligands like opba have, as a consequence, J_{MCu} values of about –30 cm^{-1}. This is a strong coupling and we can expect a similar value for **1**. In contrast, the interchain couplings are not very effective at high temperatures since kT is considerably larger than J_a and J_b. It is well established that a purely one-dimensional system is not able to exhibit spontaneous magnetization, except at absolute zero; a magnetic transition is generally a three-dimensional phenomenon.[28] For **1**, the structural changes in the crystalline phase transition are small and not sufficient to increase the interactions along the a or b axes to lead to a magnetic transition.

Conclusions

The ferrimagnetic chain [CoCu(opba)$(DMSO)_3$] (**1**) has been synthesized and characterized. It presents two crystalline phases – *Pnam* at room temperature and $Pna2_1$ at 100 K – whose structures consist of ordered infinite linear chains running along the c axis with adjacent Co^{II} and Cu^{II} ions bridged by oxamato groups. In the **α-1** phase, the DMSO molecules are disordered over the Co^{II} and Cu^{II} coordination sphere, whereas at low temperatures this structural disorder vanishes. The crystalline phase transition has been confirmed by a study using linear birefringence in a small single crystal with no polished surfaces. In addition, the LB results show a large thermal hysteresis associated to the structural changes in **1**, thereby revealing that the structural phase transition is a first-order process.

Magnetic studies (dc and ac) have been performed for **1** in a polycrystalline sample. At high temperatures, the stronger interactions along the c direction are responsible for the ferrimagnetic behavior. Since the changes that occur in the structural phase transitions do not affect this coupling significantly, anomalies in the magnetic data at the same temperatures observed by X-ray diffraction and LB measurements were not detected. The bimetallic chains in **1** are almost isolated from each other. The intrachain interaction between nearest neighbor ions is rather large but the interchain interactions are negligibly small. It is possible that **1** presents only a ferrimagnetic behavior, with correlation length increasing with a decrease of temperature without divergence of these values until the magnetometer temperature limit. In view of the crystalline arrangement, interactions along the packing direction (a axis) probably take place while the interactions along the b axis must be very weak. Therefore, the magnetic behavior for **1** below 2 K, where the effective spin of Co^{II} ions is 1/2, needs to be better investigated.

Compound **1** exhibits some interesting features with respect to magnetic nanowires. Indeed, good candidates to present slow relaxation of the magnetization and hysteretic effects require strong anisotropy, ferromagnetic intrachain coupling or ferrimagnetic behavior, and the chains must be rather isolated. Therefore, the control of the chemistry, including supramolecular aspects, of compound **1** and related systems gives rise to a challenge: the preparation of oxamato-based nanowires, and also 2D systems, with higher blocking temperatures. We are presently focusing ours efforts in this direction.

Experimental Section

Preparation of [CoCu(opba)(DMSO)$_3$] (1): Compound **1** was prepared by adding $Co(NO_3)_2 \cdot 6H_2O$ (15 mg, 0.05 mmol), previously dissolved in DMSO (3 mL), to a solution of $Na_2[Cu(opba)] \cdot 3H_2O$[15] (170 mg, 0.41 mmol) in DMSO (22 mL) whilst stirring. The crystals obtained after three months under controlled temperature (35 °C) were separated by filtration, washed with DMSO, and dried in a desiccator. Yield: 105 mg (29%). $C_{16}H_{22}CoCuN_2O_9S_3$ (605.01): calcd. C 31.76, H 3.64, Co 9.74, Cu 10.50, N 4.63, S 15.91; found C 30.80, H 3.46, Co 9.64, Cu 9.90, N 4.93, S 15.52. IR (KBr): $\tilde{\nu}$ = 3450 cm^{-1} (vs), 1610 (vs), 1575 (s, br), 1475 (m), 1400 (m), 1350 (m), 1025 (s), 940 (m), 750 (m), 575 (w), 550 (w), 450 (m).

X-ray Crystallographic Study: A blue prismatic crystal of dimensions $0.03 \times 0.08 \times 0.09$ mm^3 was used for data collection. The X-ray diffraction data were collected at 298 and 100 K on an Enraf–Nonius Kappa-CCD diffractometer with graphite-monochromated Mo-K_α radiation (λ = 0.71073 Å) up to 50° in 2θ, with a redundancy of 4. The final unit-cell parameters were based on all reflections. The temperature was controlled with an Oxford Cryosystem low temperature device. Absorption corrections were carried out using the multi-scan method.[29] The structures were solved by direct methods with SHELXS-97.[30] The models were refined by full-matrix least-squares procedures on F^2 using SHELXL-97.[31] The H atoms of the phenyl and methyl groups were positioned stereochemically and they were refined with fixed individual displacement parameters [U_{iso}(H) = 1.2 U_{eq}(C_{phenyl}) or 1.5 U_{eq}(C_{methyl})] using the SHELXL riding model. Crystal data, data collection procedures, structure determination methods and refinement results are summarized in Table 2.

CCDC-272758 (for **α-1**) and -231896 (for **β-1**) contain the supplementary crystallographic data for this paper. These data can be obtained free of charge from The Cambridge Crystallographic Data Centre via www.ccdc.cam.ac.uk/data_request/cif.

Optical Measurements: The single crystal optical characterization, namely linear birefringence (LB) and linear dichroism (LD), was done at room temperature, under incoherent light, using an Olympus model BX50 optical microscope equipped with an Olympus SC35 camera. The temperature dependence of the birefringence was investigated using a lock-in null detector technique applied for LB.[32] The equipment consists of a photoelastic modulator working at 50 kHz and a computer-controlled Soleil–Babinet compensator, with resolution of $\delta(\Delta n) \leq 3 \times 10^{-8}$, corresponding to a phase difference of about 0.01°. The system has a built-in microscope to allow the study of small samples.[33] The typical dimensions of the samples studied in this paper were a thickness of 0.1 mm and 0.25×0.50 mm^2 transverse dimensions. Due to the reduced dimensions of the crystals, no polishing procedure was possible. A pinhole inserted into the microscope allows it to choose the best regions on the surface of the sample. Measurements were made at the 488-nm line of an argon ion laser. The sample containing a drop of the mother solution where the crystal was grown was placed on a thin glass plate. Thermally conducting glue was used to connect the glass plate to the sample holder, which was inserted into an evacuated cryostat, horizontally positioned, and cooled by helium flux. When the mother solution had evaporated, the crystals were fixed to the glass plate by surface tension. The sample was oriented in the crystallographic *ac* plane. The data were collected from 295 to 20 K. The cooling and heating rates were kept to be approximately 1 K min^{-1}. The chosen orientation of 45° maximizes the birefringence.[23]

Magnetic Measurements: The dc magnetic properties of **1** were studied in a Quantum Design SQUID MPMS XL7 in the 2–300 K temperature range using polycrystalline samples. The ac magnetic properties were studied in a commercial Quantum Design PPMS system. The diamagnetic corrections were estimated from Pascal's tables.

Supporting Information (see footnote on the first page of this article): Single-crystal photographs showing LB and LD properties at room temperature.

Acknowledgments

This work was supported by CNPq, CAPES, FAPEMIG, and FAPESP. The authors thank Dr. L. Ghivelder for ac measurements. We also thank the Instituto de Nanociências CNPq/MCT and FAPESP for a postdoctoral fellowship to one of us (ACD).

[1] J. S. Miller, J. C. Calabrese, A. J. Epstein, R. W. Bigelow, J. H. Zang, W. M. Reiff, *J. Chem. Soc., Chem. Commun.* **1986**, 1026–1028.
[2] Y. Pei, M. Verdaguer, O. Kahn, J. Sletten, J. P. Renard, *J. Am. Chem. Soc.* **1986**, *108*, 7428–7430.
[3] J. S. Miller, A. J. Epstein, *Angew. Chem. Int. Ed. Engl.* **1994**, *33*, 385–415.
[4] J. M. Manriquez, G. T. Yee, R. S. McLean, A. J. Epstein, J. S. Miller, *Science* **1991**, *252*, 1415–1417.
[5] S. Ferlay, T. Mallah, R. Ouahès, P. Veillet, M. Verdaguer, *Nature* **1995**, *378*, 701–703.
[6] H. O. Stumpf, L. Ouahab, Y. Pei, D. Grandjean, O. Kahn, *Science* **1993**, *261*, 447–449.
[7] G. De Munno, M. Julve, F. Nicolò, F. Lloret, J. Faus, R. Ruiz, E. Sinn, *Angew. Chem. Int. Ed. Engl.* **1993**, *32*, 613–615.
[8] J. A. Real, A. B. Gaspar, V. Niel, M. C. Muñoz, *Coord. Chem. Rev.* **2003**, *236*, 121–141.
[9] R. Clérac, S. O'Kane, J. Cowen, X. Ouyang, R. Heintz, H. H. Zhao, M. J. Bazile, K. R. Dunbar, *Chem. Mater.* **2003**, *15*, 1840–1850.
[10] G. Christou, D. Gatteschi, D. N. Hendrickson, R. Sessoli, *MRS Bull.* **2000**, *25*, 66–71.
[11] D. Gatteschi, R. Sessoli, *J. Magn. Magn. Mater.* **2004**, *272–276*, 1030–1036.
[12] E. Coronado, J. R. Galán-Mascarós, C. J. Gómes-García, V. Laukhin, *Nature* **2000**, *408*, 447–449.
[13] S. S. Turner, D. Pevelen, P. Day, *Synth. Met.* **2003**, *133*, 497–500.
[14] A. Dei, D. Gatteschi, C. Sangregorio, L. Sorace, *Acc. Chem. Res.* **2004**, *37*, 827–835.
[15] H. O. Stumpf, Y. Pei, O. Kahn, J. Sletten, J. P. Renard, *J. Am. Chem. Soc.* **1993**, *115*, 6738–6745.
[16] H. O. Stumpf, Y. Pei, L. Ouahab, F. L. Berre, E. Codjovi, O. Kahn, *Inorg. Chem.* **1993**, *32*, 5687–5691.
[17] C. L. M. Pereira, E. F. Pedroso, M. A. Novak, A. L. Brandl, M. Knobel, H. O. Stumpf, *Polyhedron* **2003**, *22*, 2387–2390.

[18] M. G. F. Vaz, L. M. M. Pinheiro, H. O. Stumpf, A. F. C. Alcântara, S. Golhen, L. Ouahab, O. Cador, C. Mathonière, O. Kahn, *Chem. Eur. J.* **1999**, *5*, 1486–1495.
[19] M. G. F. Vaz, M. Knobel, N. L. Speziali, A. M. Moreira, A. F. C. Alcantara, H. O. Stumpf, *J. Braz. Chem. Soc.* **2002**, *13*, 183–189.
[20] C. L. M. Pereira, E. F. Pedroso, H. O. Stumpf, M. A. Novak, L. Ricard, R. Ruiz-Garcia, E. Rivière, Y. Journaux, *Angew. Chem. Int. Ed.* **2004**, *43*, 955–958.
[21] A. Caneschi, D. Gatteschi, N. Lalioti, C. Sangregorio, R. Sessoli, G. Venturi, A. Vindigni, A. Rettori, M. G. Pini, M. A. Novak, *Angew. Chem. Int. Ed.* **2001**, *40*, 1760–1763.
[22] Symmetry codes for phase **α-1**: [i] $x + 1, y, z$; [ii] $-x, -y + 1, z - 1/2$; [iii] $-x + 1, -y + 1, z - 1/2$; [iv] $x + 1/2, -y + 1/2, -z + 1/2$; [v] $x + 1/2, -y + 3/2, -z + 1/2$; [vi] $-x + 1/2, y - 1/2, -z + 1$; [vii] $-x + 1/2, y + 3/2, -z + 1$. Symmetry codes for phase **β-1**: [i] $x + 1, y, z$; [ii] $-x, -y + 1, z - 1/2$; [iii] $-x + 1, -y + 1, z - 1/2$; [iv] $-x + 1/2, y - 1/2, z - 1/2$; [v] $-x + 1/2, y + 1/2, z - 1/2$; [vi] $x + 1/2, -y + 1/2, z$; [vii] $x + 1/2, -y + 3/2, z$.
[23] J. F. Nye, *Physical Properties of Crystals; Their Representation by Tensors and Matrices*, Oxford University Press, **1985**.
[24] T. Oakberg, *PEM-90TM Photoelastic Modulator User Manual*, Hinds Instruments, Hillsboro, **1994**.
[25] O. Kahn, *Molecular Magnetism*, VCH, New York, **1993**.
[26] P. J. van Koningsbruggen, O. Kahn, K. Nakatani, Y. Pei, J. P. Renard, M. Drillon, P. Legoll, *Inorg. Chem.* **1990**, *29*, 3325–3331.
[27] S. Turner, O. Kahn, L. Rombardel, *J. Am. Chem. Soc.* **1996**, *118*, 6428–6432.
[28] R. L. Carlin, *Magnetochemistry*, Springer-Verlag, Berlin, **1986**.
[29] R. H. Blessing, *Acta Crystallogr., Sect. A* **1995**, *51*, 33–38.
[30] G. M. Sheldrick, SHELXS-97. *Program for Crystal Structure Resolution*, University of Göttingen, Germany, **1997**.
[31] G. M. Sheldrick, SHELXL-97. *Program for Crystal Structures Analysis*, University of Göttingen, Germany, **1997**.
[32] High Frequency Polarization Modulation Method for Measuring Birefringence: F. A. Modine, R. W. Major, E. Sonder, *Appl. Optics* **1975**, *14*, 757–760.
[33] M. A. S. Oliveira, J. Y. Gesland, L. C. Meira-Belo, U. A. Leitão, R. L. Moreira, *Phys. Rev. B* **2000**, *62*, 215–222.

Received: May 25, 2005
Published Online: November 2, 2005

